Proceedings World Geothermal Congress 2026
Calgary, Canada, June 8 – 11, 2026

New Insights into Siliceous Scaling in Geothermal Systems: A Case of Quartz, Opal-A, and Aluminum Silicate Scaling in the Olkaria Geothermal System, Kenya.

Wanyonyi Edwin[1]*, Kotaro Yonezu.[2] and Yokoyama Takushi[3]
KenGen PLC[1]*, Dept. of Earth Resource Engineering,[2], Faculty of Science Kyushu University[3]
wedwin.wafula@gmail.com

Keywords: Olkaria, Amorphous Opal-A, Alumino-silicate, ^{29}Si and ^{27}Al NMR, Concentration factor

ABSTRACT

The Olkaria geothermal project currently has an installed capacity of 799.3 MW and is operated by the Kenya Electricity Generating Company (KenGen) in Naivasha, Kenya. A comprehensive geochemical characterization of scale deposits was conducted using petrography, XRD, XRF, SEM-EDX, ^{27}Al and ^{29}Si MAS solid state NMR. The samples showed the presence of amorphous opal-A exemplified by a broad band showing moderate to intense scattering ranging from 19-30° 2θ, centered at 3.6 - 4.6 Å with distinct maxima around 21.5-24.5° 2θ (~3.9 Å). Strong quartz peaks were seen at 4.26 Å (~20.8° 2θ) in the (1,0,0) lattice and at 3.34 Å (~26.6° 2θ) in the (1,0,1) lattice, sometimes accompanied by other minor peaks. From the ^{27}Al MAS NMR spectrums, sharp peaks were seen at 52.5 ppm, 52.2 ppm, and 56.3 ppm, as well as small minor peaks at 12.9 ppm, 3. 9 ppm, and 16.5 ppm relative to $[Al(H_2O)_6]^{3+}$, suggesting that aluminum ions were substantially present as 4-coordinate species, but minor amounts of 6-coordinate species also existed. The mechanism for quartz precipitation is that monosilicic acid or monosilicate ion is adsorbed on the surface of a solid, and the critical nucleus of quartz is formed and grows to crystalline quartz by continuous adsorption of $[Si(OH)_4]$ or $[Si(OH)_3O^-]$ by homogenous nucleation. Amorphous aluminosilicates form as the fluid flashes to > pH 9, and a rapid reaction between $[Si(OH)_4]$ or $[Si(OH)_3O^-]$ and $[Al(OH)_4]^-$ occurs to form opal-A.

1 INTRODUCTION

The Olkaria geothermal field has exhibited a high potential for geothermal generation with the current installed capacity of 799 Mwe. A significant concern affecting the further exploitation of this resource, like in many other places, is the precipitation of scales in the circulated fluid, mainly amorphous silica (Mroczek et al., 2000; Gunnarsson and Arnórsson, 2005). Different forms of scale deposits have been reported at various parts of the generation systems, including at separators, two-phase pipelines, and even in wellbores not only in Olkaria but in other fields as well (Opondo, 2007; Zarrouk, 2014; Mroczek, 2017, Grant, et al., 2020). Aramaki et al. (2005) have discussed the prominence of silica scales containing large amounts of smectite from some geothermal regions in Japan, linked to the mixing of acidic and neutral waters with high magnesium leading to the formation of montmorillonite-like deposits together with the silica scales. Yokoyama et al. (1993) reported on the deposition of aluminum-rich scales attributed to the enrichment of Al from geothermal water into the scales. As was seen by Iler (1973) and by experiments by Gallup (1997), iron and aluminum decrease the solubility of amorphous silica, thereby leading to its deposition. Swaddle (2001) discussed the possibility of aluminosilicate deposition in highly alkaline solutions. Harder and Flehming (1970) have reported on the possibility of quartz deposition in hydrothermal solution through nucleation in the suspension of Fe $(OH)_3$ or Al $(OH)_3$ and can eventually nucleate and grow where enough impurities suppress the action of saturated monosilicic acid on the quartz surface.

Given these extraneous circumstances that engulf the deposition of minerals in geothermal systems, the purpose of this work was to characterize the scale deposition at the present mode of operation in the Olkaria geothermal field with an emphasis on their association with the characteristics of the geothermal water with the understanding that the nature of the deposits will be highly defined by the nature of the geothermal water as well as the guiding processes during deposition.

2 THE OLKARIA GEOTHERMAL FIELD

The Olkaria geothermal field is a 202 km^2 geothermal area divided into several development sectors. Within these sectors, electricity production is currently being done at Olkaria East, Olkaria Northeast, and Olkaria domes, even though more than 300 wells have been drilled in the entire geothermal project area. (Karingithi, 2000, and Opondo, 2007) Have described the orientation of these sectors and the general characteristics of the Olkaria geothermal field. The Olkaria geothermal project currently generates 799 Mwe using the conventional

single-flash system power plants and small geothermal wellhead units that also operate using the single-flash system. Currently, the system is designed to ensure nearly 100 percent hot reinjection where separated brine is connected directly to the hot reinjection wells. Scaling has been seen in several locations in Olkaria, mainly at separator stations, silencers, and, in some instances, two-phase pipelines. Slight scaling has also been seen on the main hot reinjection lines, while extensive corrosion has been experienced on the cold reinjection wells due to the injection of acidic condensate. Figure 1 shows the current system configuration where multiple wells share separators and a pictorial example of this arrangement.

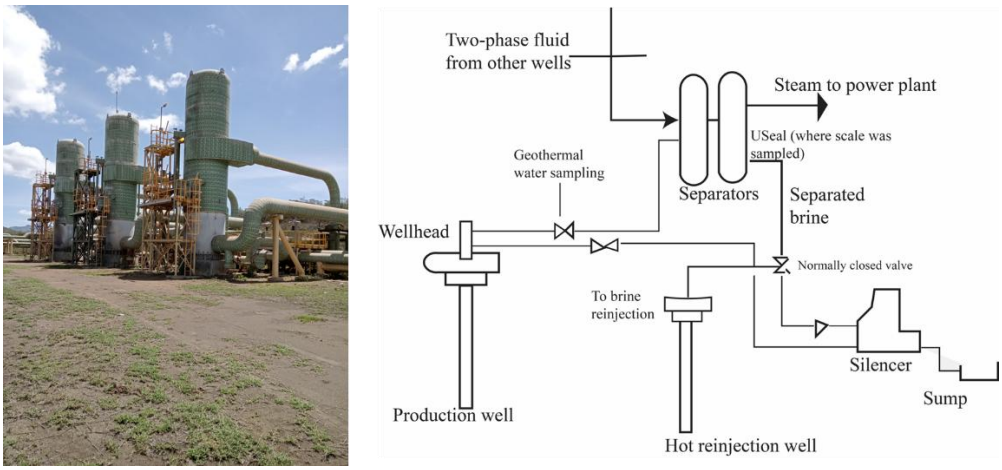


Figure 1. A photograph of one of the multiple separators, SD3 station showing the arrangement of multiple separator design. The schematic figure of the steamfield system is also shown.

3 METHODOLOGY

3.1 Sampling

For this study, scale samples were studied that formed at separators and silencers at different wells, representing several sites that were associated with these deposits. There are some inherent differences in the characteristics of the samples from the two sites. At the separators, the samples were mainly deposited at the lower sections, where the brine exited the separators and were removed during routine maintenance works in these sites. In the silencers, the scales covered the entire inner circumferences of the cylindrical-shaped silencers. In addition, geothermal water was collected from the two-phase pipeline of individual wells before separation based on the sampling and treatment method of Ólafsson and Armansson (2006). Since the current system in Olkaria allows for several wells to be separated into a singular separator, in such a situation, we determined the geothermal water from mixing the well chemistry of the individual wells feeding into such a separator.

3.2 Analysis

The mineralogical characteristics of the scale samples were analyzed by X-ray powder diffraction (XRD) using a Rigaku Ultima IV XRD machine under Cukα radiation (λ=0.15405 nm), working voltage 40 kV, current rate 20 mA at 2θ range 0-90° and 0-65°. The chemical analysis of the scale samples was done by X-ray fluorescence (XRF) using a Rigaku ZSX Primus IV XRF machine. Microscopic analysis of the polished sections was done under reflected light with a Nikon Eclipse LV100 POL polarizing microscope. Elemental mapping of the identified minerals from the polished sections was done using the Hitachi SU3500 Scanning Electron Microscope (SEM) equipped with an EDAX Octane Plus Energy Dispersive X-ray Spectroscope (EDS). To elucidate the polymerization structure of Si and coordination structure of Al in the scale samples, high-resolution solid-state ^{29}Si and ^{27}Al MAS NMR (magic angle spinning nuclear magnetic resonance) was done on a JEOL DELTA 400 NMR spectrometer. The operating frequencies for ^{29}Si and ^{27}Al were 79.43 and 104.17 MHz, respectively. The ^{29}Si were obtained at an acquisition time of 10.24 ms and a relaxation delay of 5s. The ^{27}Al MAS NMR spectra were obtained at an acquisition time of 20.48 ms and a relaxation delay of 0.5s. The rotation frequency of the zirconia sample tube was 15kHZ. The chemical shift for ^{29}Si and ^{27}Al was relative to Tetramethyl silane (TMS) and Al $(H_2O)^{3+}_6$ as an external standard. The water and steam analysis followed the methods of Arnórsson et al. (2006). Geochemical modeling was conducted with the help of The WATCH speciation program version 2.4 (Bjarnason, 2010), SOLVEQ-XPT with its SOLTHERM-XPT database (Reed et al., 2012), PHREEQC (Parkhurst and Appello, 1999) using the llnl.dat thermodynamic database and the Geochemist's Workbench© with thermo.dat database.

4 RESULTS

4.1 Properties of Geothermal Water

All the samples for chemical analysis were collected from the two-phase sampling point using a Webre separator at temperatures ranging from 150°C to 200°C. To get the final chemistry in the separator with multiple wells, a mixing was conducted using the Geochemist workbench. In terms of the temperature of operation, the separators are operating at a temperature of 150-190°C depending on the site, while the silencers are technically at an atmospheric temperature of about 90°C, but the actual fluid temperature could be higher or closer to the separator temperature as the distance between separator and silencer is very short. The reservoir temperature of the geothermal fluid for the production wells is between 250-350°C. The discharge enthalpy of the liquid is very high, between 2100 to 2600 kJ/kg, meaning that the level of boiling and steam fraction would also be high and that very concentrated geothermal water is being discharged from the wells. These geothermal waters were typically highly alkaline of sodium chloride type with a pH between 8.5 and 10.2. Generally, the salinity of these geothermal waters was below 2000 ppm but contained large amounts of silicic acid in the range of 500-1500 ppm, with Na and Cl as the other significant elements contributing to an average ionic strength of 0.1.

4.2 Petrographic Analysis of the Scales

Figure 2 shows representative photomicrographs of scales that were retrieved from separators as well as from inside silencers during regular maintenance. The scales retrieved from the separators were similar in texture and morphology, occurring as sheets of plate that were cemented together into homogenous aggregates creating foliation textures. The foliated laminae seem to have occurred first as friable aggregates before they were subsequently cemented into hard coherent deposits, probably by a secondary mechanism. The dark grey surfaces had minor equant arrangements of microcrystalline quartz grains that occurred as uniformly oriented anhedral grains. The scales from these flash separators had notable magnetism, indicating probably a significant concentration of Fe-rich components in them. A slight difference between a sample from a single well separator and a multiple well separator was that the former had a platy structure that was very thin in thickness with very sharp edges and transformed into a ball-like shape. These foliation textures are probably related to turbulence caused by differential mass flow and temporal pressure changes that could occur at the separator.

The scales retrieved from the silencers were dense, milky-looking, massive, coarse-grained deposits with micro-botryoidal appearances with visible colloid joining occurring within them. The samples showed no evidence of any stratification but slight signs of deposition in phases, as evidenced by massive layers deposited on each other. The interstitial spaces were filled with grey, fine-grained disseminations with an amygdaloidal-like appearance. The upper surface of the scales that were probably in last contact with the fluid was covered by a grey-green fine-grained substrate with a metallic luster, suggesting post-depositional oxidation on the surface.

Both sets of samples had some form of uniform direction characteristic of a response to the unidirectional flow of fluid. From the petrographic analysis of the polished sections, amorphous silica, magnetite, and some Sulfide minerals were identified. The amorphous silica occurred in two types; the first was deposited as a mottled amorphous silica and was darker, while the latter deposit was smooth with a flowing texture that seemed to fill the interstitial spaces between the mottled amorphous silica.

4.3 Mineralogical Composition of the Scales

The presence of constituent minerals was estimated from the peak intensities from XRD. Figure 3 shows the XRD spectrums of the samples collected from the separators. The samples showed the presence of amorphous opal-A exemplified by a broad band showing moderate to intense scattering ranging from 19-30° 2θ, centered at 3.6 - 4.6 Å with distinct maxima around 21.5-24.5° 2θ (~3.9 Å). Strong quartz peaks were seen at 4.26 Å (~20.8° 2θ) in the (1,0,0) lattice and at 3.34 Å (~26.6° 2θ) in the (1,0,1) lattice, sometimes accompanied by other minor peaks. Pure amorphous silica is known to occur at ~ 23° 2θ, with this shift in the range being used as an identifier for aluminum-rich opal-A (Manceau et al., 1995). Magnetite was the only iron oxide mineral identified, while weak intensities of wurtzite were also identified. A very strong peak of boehmite was identified in the sample from the OW 924 separator, which also had the highest Al_2O_3 content from XRF analysis. Weak peaks of sphalerite were also identified in the SD3 separator sample, as well as peaks of the magnesium silicate antigorite. The presence of aluminum-silicate minerals was noted in the scale samples by peaks of the zeolite natrolite in the scale sample from the silencer at OW 914B, while peaks of another zeolite, gobbinsite (which is a calcium sodium potassium aluminum silicate) were also identified in the SD3 scale sample. The samples from the separator and silencers had mild peaks for nontronite, a member of the smectite group. Peaks of Beta, BCC Ti, Alpha, and BCC Fe were also present in the silencer samples as well as separators 709 and 924. These materials usually have properties that make them useful for constructing high-pressure materials and could be related to scale impurities from the pipeline material attached to the scale deposits.

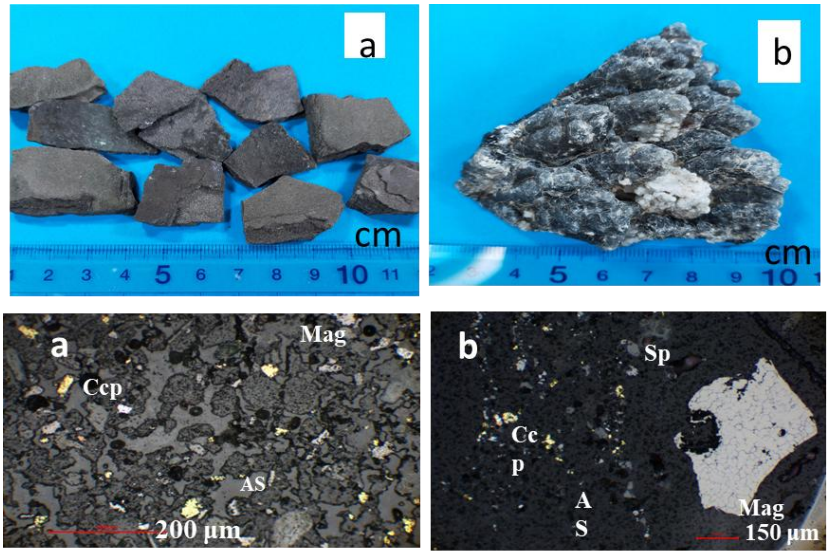


Figure 2. Photomicrographs of some of the retrieved scale samples and the accompanying reflected light photomicrographs from polished section. (a) SD3 separator and (b) OW 915C silencer (Ccp-Chalcopyrite, Mag-magnetite, AS-amorphous silica, Sp-sphalerite).

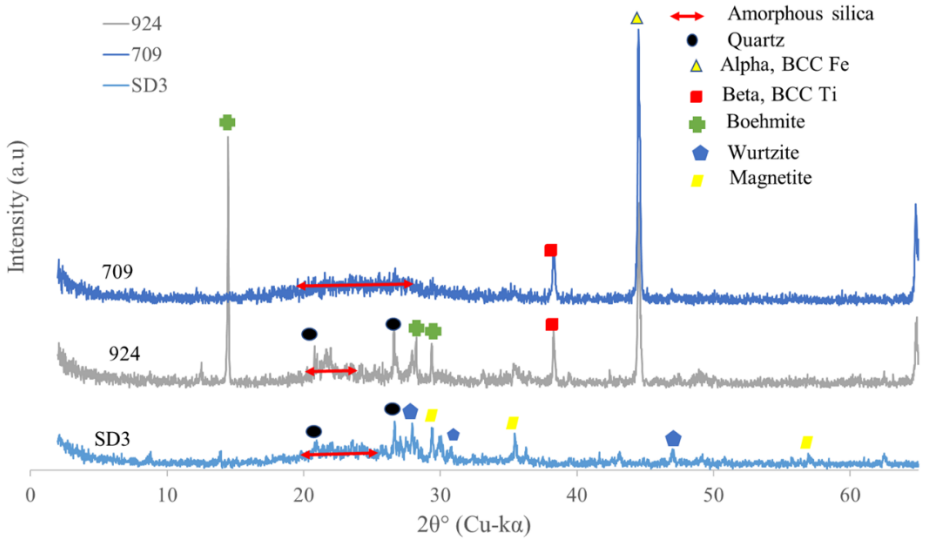


Figure 3. XRD spectrums of scale samples from the separators OW 709, SD3 and OW 924.

4.4 Chemical Composition of the Scales

The highest SiO_2 concentrations were in the samples from the silencers, 85.6 – 90.7 wt. % while in the separators ranged 65.0 – 75.0 wt.%. The second most abundant oxides were Al_2O_3, 6.5 -11.23 wt. % and Fe_2O_3 up to 16.6 wt. %. The concentration of these oxides was highest in the separators, but in the silencers, it was low, less than 0.4 wt.% for Al_2O_3 and about 2 wt.% for iron.

Most of the high iron content was found in scale samples with abundant magnetite and chalcopyrite. Na_2O and K_2O were slightly significant, ranging from 2-4 wt. % while the other oxides were very low, below 0.2 wt. %. The content of Cu was very high, as well as Zn and Pb; this was also mostly in the separators than in the silencers. A significant concentration of fluoride, as well as chloride, was also seen in some samples that are probably related to fluoride complexes and evaporites like halite in the scale sample. The LOI was low for all the samples, ranging from 3-7 wt. %. The Al/Si atomic ratio was 0 for the silencers and ranged from 0.1-0.2 for the separator scales. Yokoyama et al. (1993) proposed a method for relating the occurrence of components between scale and geothermal water. Therefore, the concentration factor of each element from the geothermal water to silica scale was calculated using this method, whereby if the value of a specific element is above 1, then the element was concentrated from the geothermal water to the silica scale, and if it's below 1, then it was probably not

involved in the formation of silica scale. The concentration factor for Al and Fe was very large, especially for the separator scale samples, affirming that these two elements could be participating in the formation of the silica scale. Since Fe was relatively large in both the separators and silencer scales compared to Al, this could mean that its mechanism of involvement was different and maybe related to another crystalline mineral, while Al would be by isomorphous substitution. The concentration factor for Mg and Ca was also large, more so for Mg in SD3, yet the geothermal water concentration and oxide concentration of Mg were low in both cases. The XRD spectrum showed the presence of a magnesium silicate in the SD3 sample, which would confirm that this very large concentration factor was related to magnesium silicate scaling. The concentration factor for Na and K was way below one, even though they have high concentrations in the geothermal water and even higher than MgO and CaO on the scale. This means they do not actively participate in the silica scale formation.

4.5 Elemental mapping by SEM-EDX

To ascertain the chemical composition of the scale samples and to establish a relationship between the minerals identified from petrography and XRD, an SEM-EDX analysis was conducted on representative scale samples, as shown in Figure 4.

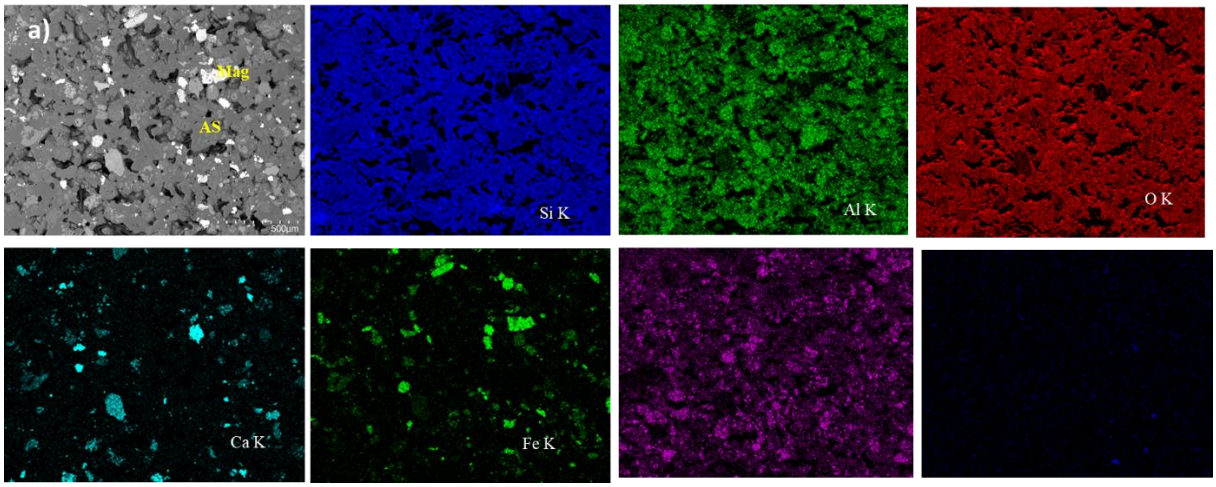


Figure 4. SEM image for SD3 silica scale sample and the elemental map for silicon, Aluminum, oxygen, calcium, Iron, potassium and zinc.

From the backscattered electron image, the scales mostly consisted of particles sized 5-60 µm, where a globular structure of the well-cemented silica colloids was seen to traverse the whole spectra of the samples. The EDX analysis confirmed the existence of some of the minerals observed under the microscope and in XRD. As seen from petrography, amorphous silica (AS) had two versions; one was a smooth, pure amorphous silica with an average chemical composition of 60 wt. % Si and 40 wt. % O, while the other had an uneven mottled appearance in its matrix, darker in shade, with reduced Si at about 40 wt.%, Al 10-15 wt. %, 5-15 wt. % K, and 1-10 wt. % Na. The first version could represent the presence of pure opaline silica, while the latter could signify the presence of aluminum silicates. Iron-rich magnetite was confirmed with an average of 65-80 wt. % Fe while the Sulfides were confirmed with Cu 47.66 wt. %, Fe 10.55 wt. %, and S 25.20 wt. %. The spectrums from EDX analysis confirm that the high Fe content is related to magnetite, and with a very low Si peak here, suggesting no ionic association between Si and Fe. Other spectrum shows an association of Al with Si, which confirms the possibility of isomorphous substitution of Si with Al. The elemental maps show the high-intensity distribution of Fe on the mapped magnetite and Sulfide minerals as well as the high-intensity and uniform distribution of Al on Si.

4.6 ^{27}Al and ^{29}Si spectra of the scales

The ^{27}Al MAS NMR technique is a powerful tool to elucidate the chemical state of Al in solid, especially the coordination number (4, 5, and 6). Some researchers have measured ^{27}Al MAS NMR spectra for Al in silica scales formed from geothermal waters (Yokoyama et al., 1993, 2004; Gallup, 1997; Aramaki et al. 2005; Hinman and Kotler, 2013). Figure 5 shows the ^{27}Al NMR spectra for the OW 915C scale that had a sharp peak at 56.3 ppm and a minor peak at 16.5 ppm, suggesting that both the Al (4) and Al (6) species were present in this sample. On the other hand, the sample from OW 914A had a single sharp peak at 51.5 ppm, indicating that only Al (4) was present on this scale. As reported by Yokoyama et al. (1993), usually, there are two types of silica scales. One that could have only the Al (4) and another that could have both coordination of Al (4) and Al (6). This is usually related to different mechanisms occurring (Yokoyama et al., 2004). Since Al is uniformly distributed in the silica phase in Figure 4, the 4-coordinate aluminum ion (AlO_4 unit) is present at the silicon site (SiO_4 unit) in the silica phase by

isomorphous substitution. The 6-coordinate aluminum could be related to the presence of some aluminum silicates in the sample.

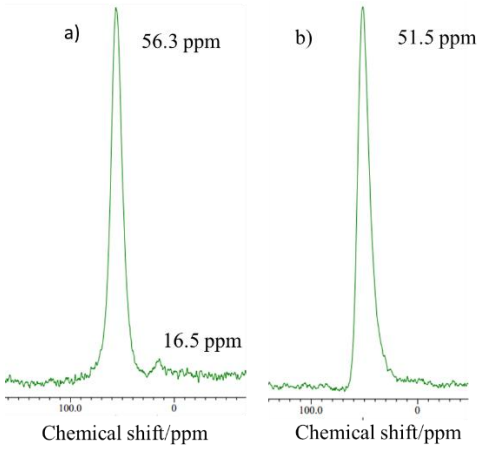


Figure 5. ^{27}Al MAS NMR spectrum a) for the OW-915C and b) OW 914A silica scale sample.

High-resolution ^{29}Si MAS NMR was applied to check the polymerization structure of silicic acid in the silica scale sample. Using NMR data, several SiO_4 units with different structures can be identified based on the number of Q units, representing silicon or aluminum atoms bonded to four oxygen atoms of a Si (Lippmaa et al., 1980). In addition, the symbol Q^n is often used where n indicates the number of other Q units attached to the tetrahedron, which can be between 0-4 units. In other cases, where there is an isomorphous substitution of Si by Al to form aluminosilicates, this is often shown as $Q^n(mAl)$, where m indicates the number of AlO_4 tetrahedra bound to the central silicon of a Q^n unit (Miyazaki and Yokoyama, 1999). Fig. 6 shows the ^{29}Si MAS NMR spectra, while Figure 7 shows the deconvoluted spectra for the same samples.

The results showed that three possible structures could be assigned to these scale samples: -111.2 to be assigned to $Q^4(0Al)$, -106.2 ppm to be assigned to $Q^4(1Al)$, and -99.5 to be assigned to $Q^4(2Al)$. Table 1 shows the assignment of these spectra. The sharp peak at -107.1 ppm was assigned to crystalline quartz. Other peaks were considered to be due to opal-A. This result corresponds to the XRD patterns in Figure 3, showing that the silica scale samples were composed of a mixture of amorphous opal-A and crystalline quartz. The broad peak width indicates that different chemical states of Si were present in the silica scale sample.

4.7 Mineral saturation state

The geothermal water is supersaturated with respect to pure amorphous silica in the silencers with saturation indices at 3 - 4.5, while at the separators, it is undersaturated. Considering the aluminum-rich conditions, the saturation indices at the separators now increase to between 1.2 and 1.8. The saturation state of quartz shows that it is supersaturated in geothermal water. Magnesium silicate peaks were identified in the sample from the SD3 separator, which also had the highest Mg enrichment factor, while OW 924 and OW 709 also had a high Mg enrichment factor. From the calculated saturation indices, the three sites were very supersaturated with respect to antigorite ($Mg_{48}Si_{34}O_{85}(OH)_{62}$ which had the highest index of all minerals in the calculation. From the XRD spectra, some aluminosilicate mineral peaks were identified as related to zeolite minerals Natrolite and gobbinsite which are of the sodium, calcium aluminum silicate stoichiometry. Hence, we evaluated the saturation state of the aluminosilicate minerals in this geothermal water. Nontronite- (Na, K, Mg, Ca) (Na_{33}, $Fe_2Al_{33}Si_3$, H_2O_{12}) was the most supersaturated mineral matching this stoichiometry, wherein the separator scales it was the second most supersaturated mineral, while in the silencer samples it was the most supersaturated mineral.

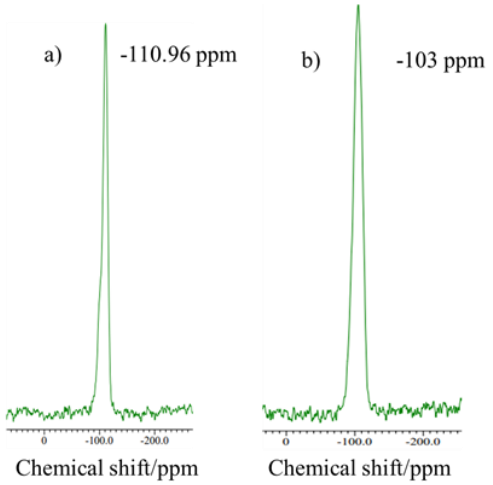


Figure 6. ^{29}Si MAS NMR spectrum a) for the OW-915C and b) OW 709 silica scale sample.

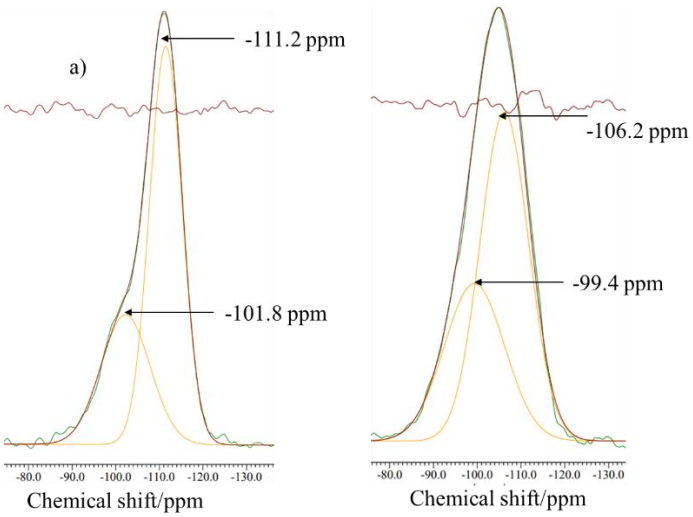


Figure 7. Deconvolution of the ^{29}Si MAS NMR spectrum for a) 915C and b) 709. The orange spectra inside the curve represents the deconvoluted spectra, green line is the simulated spectra while the brown line is the measured spectra. The wavy line on top represents the difference in intensities between the simulated and Measured spectra.

Table 1. Assignment of the ^{29}Si MAS NMR spectra

Location	OW 915C	OW 709	OW 43
Structure	Chemical shift/ppm		
$Q^4(0)$	-111.2		-109.3
$Q^4(1Al)$		-106.2	-107.3
$Q^4(2Al)$	-101.8	99.5	-102.8

5 DISCUSSION

The deposition in Olkaria was majorly siliceous, comprising amorphous opal-A scales that were aluminum-rich, with quartz also depositing of its own accord. Other minerals present included sulfides (chalcopyrite, wurtzite, sphalerite, bornite galena), magnetite as well as aluminum silicate minerals. These mineral deposits were all precipitated from the same geothermal water during production, meaning that it's possible to obtain diverse deposits emanating from the same geothermal water. The calculated saturation index from the geothermal water shows an undersaturation with respect to pure amorphous silica but a supersaturation of amorphous aluminum opal-A, quartz, and the other identified minerals. This means that silica scaling due to pure amorphous silica would not be expected to occur but silica scaling due to quartz would be expected to occur. Ichikuni (1970) reported that aluminum was incorporated in silica scales even where the concentration of aluminum in the brine was at very low levels. Yokoyama et al. (1993) reported that aluminum was concentrated into silica scales from geothermal waters during their formation. The enrichment factor of aluminum from geothermal water to silica scale was considerably high. According to the proposed chemical reaction by Gallup (1997), the formation mechanism of the silica scale in Olkaria is through reactions between $[Al(OH)_4]^-$ and $Si(OH)_3O^-$ or $Si(OH)_4$ proceeding rapidly to form an aluminum silicate suggesting that Al affected the formation of the opal-A. The reaction between $Si(OH)_4$ or $[Si(OH)_3O^-]$ and $[Al(OH)_4]^-$ occurs to form the opal-A seen in Olkaria. This reaction is expected to occur very rapidly. This amorphous silica scale may not convert to crystalline quartz for a short time because of high activation energy (Mizutani, 1966).

It has been reported that aluminum is present as an Al-Si complex in weak alkaline geothermal water (Masunaga et al., 2020). If the soluble Al-Si complexes may be easily adsorbed on the surface of the solid, the supersaturated monosilicic acid or silicate ion can rapidly combine with the adsorbed Al-Si complexes to form the type of silica scales seen in Olkaria. Quartz may be deposited directly from the Olkaria geothermal water, after the nucleation of quartz on the solid surface, monosilicic acid or silicate ion is adsorbed slowly without the participation of foreign ions such as Al^{3+}. If aluminum participates in the formation of silica scales, the crystallization of quartz may be inhibited. If monosilicic acid or monosilicate ion is adsorbed on the surface of a solid, the critical nucleus of quartz is formed and grows to crystalline quartz by continuous adsorption of $Si(OH)_4$ or $[Si(OH)_3O^-]$. This marks the beginning of the process of homogenous nucleation. Ichikuni (1969) reported the direct formation of crystalline quartz from thermal spring water.

6 CONCLUSION

The deposition in Olkaria was majorly siliceous, comprising amorphous opal-A scales that were aluminum-rich, with quartz also depositing of its own accord. The formation mechanism of the silica scale in Olkaria is through reactions between $[Al(OH)_4]^-$ and $Si(OH)_3O^-$ or $Si(OH)_4$ proceeding rapidly to form an aluminum silicate suggesting that Al affected the formation of the opal-A. If monosilicic acid or monosilicate ion is adsorbed on the surface of a solid, the critical nucleus of quartz is formed and grows to crystalline quartz by continuous adsorption of $Si(OH)_4$ or $[Si(OH)_3O^-]$.These mineral deposits were all precipitated from the same geothermal water during production, meaning that it's possible to obtain diverse deposits emanating from the same geothermal water. At present, Olkaria operates geothermal power plants generating 799 Mwe, with some of the wells currently affected by scales. This study has demystified the deposition regime, that has made the plant operators, to change the steamfield design, and also opened discussions on the possible introduction of scale inhibition.

Acknowledgements

We thank the Kenya Electricity Generating Company PLC (KenGen) for supporting this study. This research was supported by the Japan International Cooperation Agency (JICA) KIZUNA program. We also thank members of the Economic Geology laboratory at Kyushu University for fruitful discussions and members of the Olkaria Geochemistry laboratory for assistance with sample collection. We thank Ms. Keiko Ideta for helping with the NMR measurements at the Institute of Chemical Materials and Engineering, Kyushu University.

REFERENCES

Mroczek, E., Graham, D., and White, S., 2000. Deposition of amorphous silica in porous packed beds predicting the lifetime of reinjection aquifers. Geothermics, 29, 737–757.

Mroczek, E., Graham, D., Siega, C. and Bacon, L., 2017. Silica scaling in cooled silica saturated geothermal water: Comparison between Wairakei and Ohaaki geothermal fields, New Zealand. Geothermics, 69, 145–152.

Opondo, K., 2007. Corrosive species and scaling in wells at Olkaria, Kenya, Reykjanes, Svartsengi, and Nesjavellir, Iceland. UNU-GTP, Reports 2006, Number 2.

Gunnarsson, I. and Arnórsson, S., 2005. Impact of silica scaling on the efficiency of heat extraction from high-temperature geothermal fluids. Geothermics 34, 320-329.

Zarrouk, S. J., Woodhurst, B. C., and Morris, C., 2014. Silica scaling in geothermal heat exchangers and its impact on pressure drop and performance: Wairakei binary plant, New Zealand. Geothermics, 51, 445–459.

Grant, H., Hannington, M., Hardardottir, V. and Fuchs, S., 2020. Trace metal distributions in sulfide scales of the seawater dominated Reykjanes geothermal system: constraints on sub-sea floor hydrothermal mineralizing processes and metal flux. Ore Geology Reviews, 116, 103–145.

Aramaki, Y., Yokoyama, T., Okaue, Y., Imai, A. and Watanabe, K. R., 2005. A study on the formation of smectite in silica scales precipitated from geothermal waters: The effect of magnesium. Resource Geology Vol. 55, no. 3, 281 – 284.

Yokoyama, T., Sato, Y., Maeda, Y., Tarutani, T. and Itoi, R., 1993. Siliceous deposits formed from geothermal water I. The Major Constituents and the Existing States of Iron and Aluminum. Geochemical Journal, Vol. 27. pp.375-384.

Iler, R.K., 1973. Effect of dissolved alumina on the solubility of amorphous silica in water. J. Colloid Interface Sci. 43, 399-408.

Gallup, D.L., 1997. Aluminum silicate scale formation and inhibition: scale characterization and laboratory experiments. Geothermics, 26(4), 483–499.

Swaddle, T., 2001. Silicate complexes of aluminum (III) in aqueous systems. Coordination Chemistry Reviews, 219–221, 665–686.

Harder, H. and Flemming, W., 1970. Quartz synthesis at low temperatures. Geochemica et Cosmochimica Acta, 34, 3, 295-300.

Karingithi, C.W., 2000. Geochemical characteristics of the Greater Olkaria geothermal field, Kenya. Report 9 in Geothermal training in Iceland 1998. UNU-GTP, Iceland, 165-188.

Ármannsson, H., and Ólafsson, M., 2006. Collection of geothermal fluids for chemical analysis. ÍSOR – Iceland GeoSurvey, Reykjavík, report ISOR-2006/101, 17.

Arnórsson, S., Bjarnason, J.O., ¨ Giroud, N., Gunnarsson, I. and Stefansson, A.,2006. Sampling and analysis of geothermal fluids. Geofluids 6, 203–216.

Bjarnason, J.O., 2010. The chemical speciation program WATCH. Version 2.4 Iceland GeoSurvey. Accessible at. http://www.hydrothermal.is/software.

Reed, M.H., Spycher, N. F., and Palandri, j., 2012. SOLVEQ-XPT: A Computer program for computing aqueous-mineral-gas equilibria. Department of the Geological Sciences University of Oregon Eugene.

Parkhurst, D.L. and Appelo, C.A.J., 1999. User's Guide to PHREEQC (Version 2): A Computer program for speciation, batch-reaction, one-dimensional transport, and inverse geochemical calculations, Water-Resources Investigations Report 99–4259. USGS, Denver, USA, pp. 1–312.

Manceau, A., Ildefonso, P., Hazemann, J., Flank, A. and Gallup, D., 1995. Crystal chemistry of hydrous iron silicate scale deposits at the Salton Sea Geothermal field. Clays and Clay Minerals, Vol. 43, No. 3, 304-317.

Yokoyama, T., Taguchi, S., Motomura, Y., Watanabe, K., Nakanishi, T., Aramaki, Y. and Izawa, E., 2004. The effect of aluminum on the bio deposition of silica in hot spring water: Chemical state of aluminum in siliceous deposits collected along the hot spring water stream of Steep Cone hot spring in Yellowstone National Park, USA. Chemical Geology 212, 329 – 337.

Gallup, D.L., 1997. Aluminum silicate scale formation and inhibition: scale characterization and laboratory experiments. Geothermics, 26(4), 483–499.

Lippmaa E, Samoson A, Magi M., Engelhardt G., and Grimmer A., R., 1980. Structural Studies of silicates by solid-state high-resolution 29Si NMR. J Am Chem Soc 102, No.15.

Miyazaki, A. and Yokoyama, T., 1999. Effects of anions on local structure of Al and Si in aluminosilicates. J. of Colloid and Interface Science 214, 395–399.

Mizutani, S., 1966. Transformation of silica under hydrothermal conditions. J. Earth Sci. Nagoya University, 14, 56-88.

Hinman, N. W. and Kotler, J. M., 2013. Aluminum in silica phases formed in hot spring. Procedia Earth and Planetary Sci., 7, 365-368.

Ichikuni M. and Nakagawa, R., 1969. Direct formation of crystalline silica from acid thermal spring water. Bull. Chem. Soc. Jpn., 40, 2437-2439.

Ichikuni, M., 1970. Incorporation of aluminum and iron into siliceous sinters. Chem. Geol., 6, 273-279.